

Reconfigurable Filtering of Neuro-Spike Communications using Synthetically Engineered Logic Circuits

Geoffly L. Adonias^{1,*}, Harun Siljak², Michael Taynnan Barros³, Nicola Marchetti², Mark White⁴ and Sasitharan Balasubramaniam¹

¹*Telecommunications Software & Systems Group, Waterford Institute of Technology, Waterford, Ireland*

²*CONNECT Centre, Trinity College Dublin, Dublin, Ireland*

³*CBIG at Biomeditech, Faculty of Medicine and Health Technology, Tampere University, Tampere, Finland*

⁴*Research, Innovation & Graduate Studies, Waterford Institute of Technology, Waterford, Ireland*

Correspondence*:
Geoffly L. Adonias
gadonias@tssg.org

2 ABSTRACT

3 High-frequency firing activity can be induced either naturally in a healthy brain as a result of the
4 processing of sensory stimuli or as an uncontrolled synchronous activity characterizing epileptic
5 seizures. As part of this work, we investigate how logic circuits that are engineered in neurons can
6 be used to design spike filters, attenuating high-frequency activity in a neuronal network that can
7 be used to minimize the effects of neurodegenerative disorders such as epilepsy. We propose a
8 reconfigurable filter design built from small neuronal networks that behave as digital logic circuits.
9 We developed a mathematical framework to obtain a transfer function derived from a linearization
10 process of the Hodgkin-Huxley model. Our results suggest that individual gates working as the
11 output of the logic circuits can be used as a reconfigurable filtering technique. Also, as part of
12 the analysis, the analytical model showed similar levels of attenuation in the frequency domain
13 when compared to computational simulations by fine-tuning the synaptic weight. The proposed
14 approach can potentially lead to precise and tunable treatments for neurological conditions that
15 are inspired by communication theory.

16 **Keywords:** neuron, hodgkin-huxley, linear model, transfer function, systems theory, epilepsy, filter.

1 INTRODUCTION

17 Seizure dynamics with either spontaneous and recurrent profiles can occur even in healthy patients during
18 the processing of sensory stimuli or it could manifest itself as an uncontrolled synchronous neural activity
19 in large areas of the brain (Jirsa et al., 2014). Any disruption to the mechanisms that inhibit action potential
20 initiation or the stimulation of processes that facilitate membrane excitation, can prompt seizures. Tackling
21 this disease efficiently is an existing clinical issue where new approaches are constantly being investigated
22 in order to provide precise and reliable strategies in inhibiting or disrupting seizure-triggering populations

23 of neurons. For example, controlling neuron firing threshold can most likely prevent seizure activity, which
24 can often be achieved at a single neuron level (Scharfman, 2007).

25 The development of techniques for the treatment of this type of neurodegenerative disorder is challenging
26 not only due to the complexity of the brain function and structure but also as a result of the invasiveness and
27 discomfort caused by today's most common neurostimulation or surgery approaches (Rolston et al., 2012).
28 However, due to the lack of success in non-invasive approaches, the immediate future epilepsy treatment
29 will still see invasive methods. This approach must achieve population-level control with state-of-the-art
30 technology in not only neuroengineering but must also integrate other disciplines. Recent advancements in
31 nanotechnology, for instance, have been enabling the development of novel devices at the nano-scale that
32 are capable of improving bio-compatibility. Nanotechnology-based treatment also includes advantages in
33 the treatment precision, patient comfort as well as longer treatment lifetime. However, there still remain
34 numerous challenges in the use of nanotechnology. For example, the passage of chemicals through the
35 blood-brain barrier (BBB) is among the many challenges that disrupt the efficiency of nanoparticles-
36 mediated drug delivery functioning. Challenges still remain as to how nanoparticles that pass through
37 the BBB will diffuse towards specific neural populations. However, if the drug-loaded nanoparticles can
38 be delivered at sufficient concentrations and accurately to a specific location, this can influence neural
39 activities (Bennewitz and Saltzman, 2009; Veletić et al., 2019). As an example, drug delivery targets
40 specific neurodegeneration promoting factors (Feng et al., 2019) by performing a drug-induced control over
41 intracellular, extracellular and synaptic properties that regulate spiking activity (Blier and De Montigny,
42 1987).

43 Previous studies on the firing response of neurons have investigated the filtering capabilities either due to
44 realistic synaptic dynamics (Brunel et al., 2001; Moreno-Bote and Parga, 2004) or by naturally manipulating
45 the resting potential of voltage-dependent active conductances of a neuron enhancing its temporal filtering
46 properties (Fortune and Rose, 1997; Motanis et al., 2018). On the other hand, existing analyses do not
47 account for the many molecular control mechanisms that may influence the synaptic activity, e.g. drug. In
48 the case of seizures, the understanding of the drug-induced firing response may allow further analysis on
49 the impact of high-frequency firing on the neural tissue as well as how to desynchronize or slow it down.
50 Frequency-domain analysis has been performed on top of linear models of the Hodgkin-Huxley (HH)
51 formalism to investigate not only the transmission of information through the use of subthreshold electrical
52 stimulation (Khodaei and Pierobon, 2016) but also the influence of axonal demyelination on the propagation
53 of action potentials (Chaubey and Goodwin, 2016). Although Hodgkin-Huxley is not the only neuron model
54 available in the literature, it is one of the most plausible models for computational neuroscience (Long and
55 Fang, 2010). Other proposed models are, for example, integrate-and-fire, Izhikevich and Fitzhugh-Nagumo
56 models (Mishra and Majhi, 2019).

57 The manipulation of cellular activity, such as neuronal spiking activity, using molecules complexes to
58 mimic logic gates and transistors has also been proposed in the literature. One example is the work of Vogels
59 and Abbott (2005), in which the propagation of neuronal signals in networks of integrate-and-fire models
60 of neurons was investigated and they found that different types of logic gates may arise within the network
61 by either strengthening or weakening specific synapses. Goldental et al. (2014) used identical neurons
62 to propose dynamic logic gates that work based on their historical activities, interconnection profiles, as
63 well as the frequency of stimulation at their input terminals. In our previous works (Adonias et al., 2019;
64 Adonias et al., 2020), we developed several logic gates arranged in groups of three heterogeneous models of
65 neurons, with two working as inputs and one as the output, and performed a queueing-theoretical analysis
66 aiming at the study of such a complex network as a single element behaving as the collective of those

67 cells. Irrespective of the tremendous efforts from the scientific community, these works do not provide a
 68 framework of reconfigurable circuits that could pave the way for more sophisticated approaches for neuron
 69 control. Further investigation of novel neuronal electronic components constructions is needed to develop
 70 bio-compatible and reliable solutions that can address defective neuronal networks. While the scientific
 71 community has been witnessing remarkable progress in the manipulation and engineering of the behavior
 72 of mammalian cells (Lienert et al., 2014), the existing models do not yield analytical expressions that could
 73 be used to model drug-induced filtering capabilities of a neuron and, in particular, incorporating computing
 74 paradigms. The main focus of this work is to lay the ground-work of analytical models for digital filters
 75 that are designed and engineered into neurons, potentially leading to the development of novel epilepsy
 76 treatments.

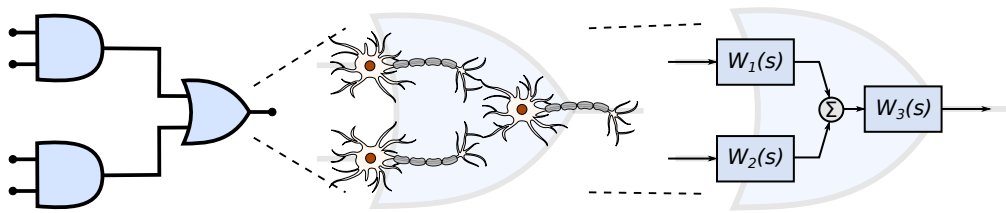


Figure 1. Engineered neuronal digital logic circuit, where each gate is composed of three neurons and each block $W_i(s)$ represents one neuron as a transfer function to enable communication metric analysis .

77 In this work, we propose a mathematical framework aiming at the interpretation of the filtering capabilities
 78 in small populations of neurons that are engineered into a logic circuit (Figure 1). The circuit aims to
 79 reduce the firing rates from its inputs by performing the binary logic as well as integrating reconfigurability,
 80 where the different logic circuit arrangements, as well as logic gate types, can be tuned to change the
 81 filtering properties. To achieve that in our mathematical framework, we modify parameters on the logic
 82 circuit transfer function, derived from the linear interpretation of the Hodgkin-Huxley neuronal model.
 83 These parameters are related to neuronal and synaptic properties of a neuro-spike communication, such
 84 as conductances and weight, and can potentially be achieved through the sustained administration of a
 85 specific drug. Our mathematical framework is, from an application point-of-view, a design platform for
 86 neuroscientists in creating filtering solutions for smoothing out the effects of neurological diseases that
 87 require the minimization of firing activity. The framework models the effects of drug-induced molecular
 88 changes in models of neurons aiming to control the neuronal activity of a synthetic engineered cell, however,
 89 the fabrication and specifications of such a drug are out of the scope of this paper. The contributions of this
 90 paper are as follows:

- 91 • **Neuronal logic circuits are built** using computational models of neurons and this arrangement is
 92 expected to be capable of acting as digital filters, converging four inputs into one output with a shift in
 93 attenuation driven by modifications to the synaptic weight.
- 94 • **A mathematical framework is proposed** paving the way for the design of neuronal digital filters to
 95 help suppress the destructive effects of neurodegenerative diseases. This framework should enable
 96 the relationship between biophysical models and drug design, facilitating scientists control over the
 97 behavior of the filters.
- 98 • **Analysis of the performance of the neuronal filters** in terms of accuracy and of signal power
 99 attenuated by the circuit. This analysis gives an insight into how parameters such as weight or
 100 frequency at the input would affect the performance of such filters.

101 The remainder of this paper is as follows, Section 2.1 briefly describes how neurons differ between each
102 other and how they communicate with one another. In Section 2.2, we explain how neurons can function
103 as non-linear electronic circuits based on the seminal work of Hodgkin and Huxley (1952) and we also
104 describe the process of linearization aiming to derive a transfer function of the filter model. The filter
105 design is explained in Section 2.3 which also covers how neurons are represented as compartments and
106 connected to form logic gates and, consequently, to form logic circuits. In Section 3, we present the results
107 that are discussed in Section 4 and, finally, the conclusions are presented in Section 5.

2 MATERIAL AND METHODS

108 2.1 Neuronal Communication

109 To be able to synthetically implement complex functions inside the brain, we must control how the
110 neurons exchange information using the propagation of action potentials inside a network of neurons. The
111 number of excitatory and inhibitory connections between neurons determines the spatio-temporal dynamics
112 of the action potentials propagation (Zhou et al., 2018). Efficient coding and modulation of neuronal
113 information have been used to implement bio-computational approaches in our previous work (Adonias
114 et al., 2020). Bio-computing can be created from neuronal networks that are engineered to function as logic
115 circuits through controlling the neuro-spike communication and curbing the signal propagation dynamics
116 between the neurons.

117 We aim to investigate the neuronal and synaptic properties in constructing logic circuits that perform the
118 filtering of spikes in small populations from the somatosensory cortex. The cortex is responsible for most
119 of the signal processing performed by the brain and comprises a rich variety of morpho-electrical types of
120 neuronal and non-neuronal cells. We will take into account these characteristics in the construction of our
121 mathematical framework that is used to design the circuits.

122 2.1.1 Properties of a Neuron

123 Neurons are divided into three main parts: dendrites, soma and axon. Dendrites receive stimuli from other
124 cells and the way these dendritic trees are projected onto neighboring neurons in a network helps to classify
125 neuron morphological types. The axon passes stimuli forward to cells connected down the network through
126 its axon terminals and the soma is the main body of the neuron. Each neuron's response to a stimulus will
127 dictate the electrophysiological neuron type. The soma is where most proteins and genes are produced and
128 where stimuli are generated and fired down the axon.

129 Besides the way dendrites are projected, the proteins and genes that neurons express and their
130 morphological and electrophysiological characteristics are important for the classification of different
131 types of neurons. One of the most comprehensive works on neuronal modelling, by Markram et al. (2015),
132 classifies the neurons from the rat's somatosensory cortex based on their morpho-electrical properties
133 (morphological and electrical characteristics) as well as the cortical layer they belong (columnar and
134 laminar organization).

135 2.1.1.1 Morpho-electrical Characteristics

136 Even though all neurons used in this work can assume different morphological structure, it is exactly by
137 analyzing their axonal and dendritic ramification that we can have a good enough categorization of their
138 respective morphological types. Regardless of their types, neurons in the cortical layer are considered of
139 small sizes (8 - 16 μm). Furthermore, inhibitory neurons can be better identified by their axonal features

140 while excitatory neurons can be more easily classified based on their dendritic features (Markram et al.,
141 2015). Each morphological type (m-type) can fire different spiking patterns and this may affect the gating
142 capabilities of neurons due to the fluctuations on precise spike timing. Markram et al. (2015) categorized
143 11 different electrical types (e-types) of neurons, hence, 11 different ways of firing a spike train generated
144 in response to an injected step current.

145 **2.1.1.2 Cortical Organization**

146 The cerebral cortex comprises six distinguished horizontal layers of neurons, with each layer having
147 particular characteristics such as cell density and type, layer size and thickness. This horizontal
148 configuration is also known as a “laminar” organization, where the layers are identified as (1) Molecular
149 layer, which contains only a few scattered neurons and consists mostly of glial cells and axonal and
150 dendritic connections of neurons from other layers; (2) External granular layer, containing several stellate
151 and small pyramidal neurons; (3) Pyramidal layer, contains non-pyramidal and pyramidal cells of small
152 and medium sizes; (4) Inner granular layer, predominantly populated with stellate and pyramidal cells,
153 this is the target of thalamic inputs; (5) Ganglionic layer, containing large pyramidal cells that establish
154 connections with subcortical structures; and (6) Multiform layer, populated by just a few large pyramidal
155 neurons and a good amount of multiform neurons, which sends information back to the thalamus. All
156 layers may contain inter-neurons bridging two different brain regions.

157 The neurons are not just stacked one on top of another suggesting a horizontal organization, indeed
158 vertical connections are also found in between the neurons from either the same or different layers. This
159 allows another type of classification known as mini-columns (also called, micro-columns) with a diameter
160 of 30 - 50 μm and when activated by peripheral stimuli, they are seen as macro-columns, with a diameter
161 of 0.4 - 0.5 mm (Peters, 2010). This will create network topologies with intrinsic characteristics, e.g.
162 connection probabilities between neurons, that influence the signal propagation to converge into either a
163 specific pattern or flow.

164 **2.1.2 Neuron-to-neuron Communication**

165 The communication between a pair of neurons is done through the diffusion of neurotransmitters in
166 the synaptic cleft; this process is triggered by an electrical impulse reaching the axon terminals of the
167 transmitting cell characterizing an electrochemical signalling process known as the *synapse*. Action
168 potentials propagate down the axon of the pre-synaptic cell, which is the sender cell, and when reaching
169 the axon terminals also known as pre-synaptic terminals, it triggers the release of vesicles containing
170 neurotransmitters into the synaptic cleft, which is the gap between a pre- and a post-synaptic terminal,
171 as illustrated in Figure 2. Those neurotransmitters will probabilistically bind to neuro-receptors located
172 at the post-synaptic terminals, i.e. dendrites (Balevi and Akan, 2013), triggering the exchange of ions
173 through the membrane that can either excite or inhibit the cell, depending on the type of neurotransmitters
174 that were received. In our work, we focus on the synaptic weight between the pre- and post-synaptic
175 terminals. The synaptic weight is a measure of how much influence the pre-synaptic stimuli have on
176 the post-synaptic cell and it is known to have its value best approximated to the time integral of the
177 synaptic conductance (Gardner, 1989). Furthermore, the value of synaptic conductance in the post-synaptic
178 terminal is driven by the number of neurotransmitters bound to neuroreceptors (Guillamon et al., 2006).
179 We illustrate the synaptic weight, in Figure 2, as red neurotransmitters which should have their release
180 from the pre-synaptic terminals induced by the administration of a specific drug.

181 In an excitatory synapse, the membrane potential of the post-synaptic cell, which rests at approximately
182 -65 mV, will start depolarizing itself until it reaches a threshold, th , for action potential initiation. On the

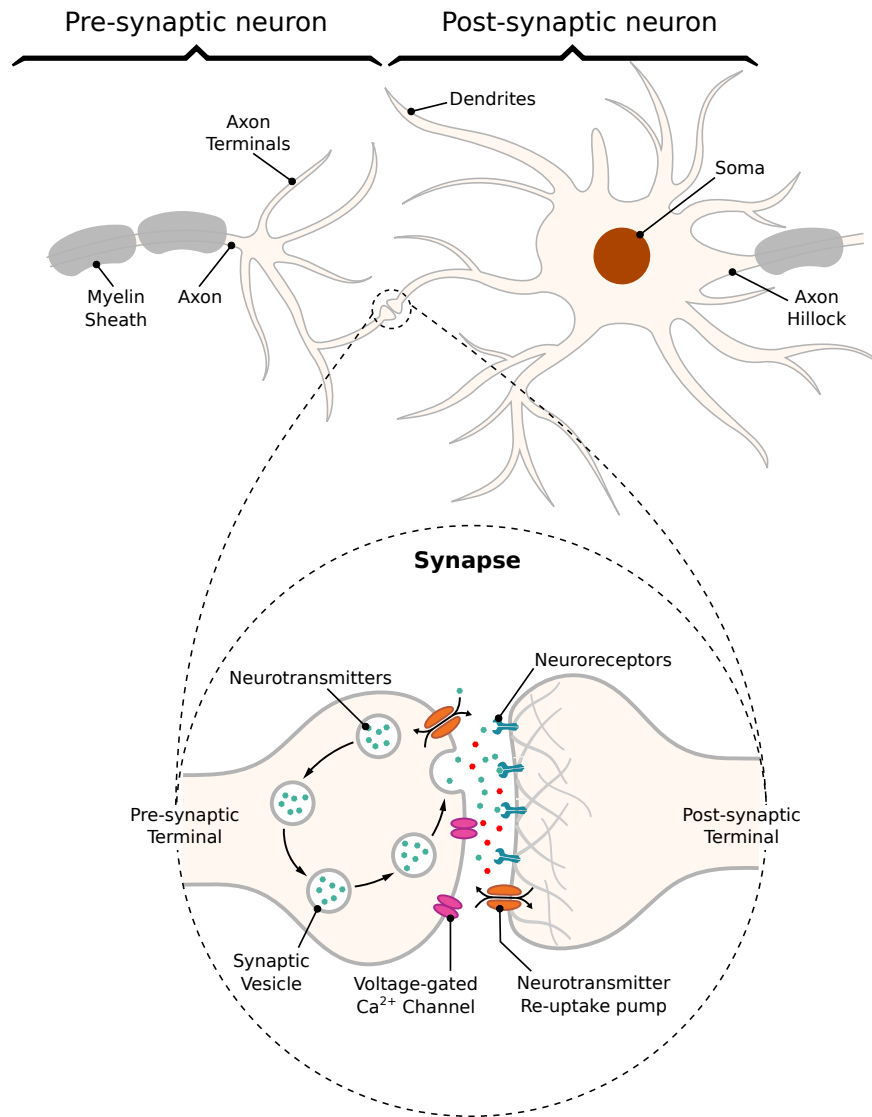


Figure 2. Schematic of a *synapse*; action potentials traveling down the axon trigger the release of neurotransmitters into the cleft between pre- and post-synaptic terminals, traveling towards neuroreceptors on the other end leading to changes on membrane conductance that can either excite or inhibit the post-synaptic neuron.

183 other hand, if the synapse is inhibitory, the membrane should get even more polarized making it nearly
 184 impossible for the cell to fire a spike and not allowing the propagation of any signal down the network
 185 from the inhibited cell. After reaching *th*, the membrane potential should increase towards a maximum
 186 peak of depolarization, and then the cell will start the process of repolarization towards its resting potential.
 187 For a brief moment, the potential inside the cell will cross the level of potential when at rest making
 188 the membrane hyperpolarized, which is a period known as the *refractory period* and it can be further
 189 subdivided as *absolute* and *relative*. The absolute refractory period (ARP) lasts around 1 - 2 ms during
 190 which the neuron is unable to fire again regardless of the strength of the stimuli; then, it is followed by
 191 the relative refractory period (RRP) during which a response in the potential of the cell may be evoked
 192 depending on the strength of the stimuli (Mishra and Majhi, 2019).

193 2.2 Electronic Interpretation of a Neuron Model

194 The main structures of a neuron, previously mentioned in Section 2.1.1, can assume different shapes and
 195 spatial structures that play an important role in determining its input and output relationship. By sectioning
 196 the neuron into several compartment models, we are able to account for the influence that individual
 197 compartments have on the communication process of the neuron. Even though we consider the same
 198 value of resting potential for all compartments of the cell, there is some discussion on whether different
 199 compartments have different potentials when at rest (Hu and Bean, 2018).

200 We aim to develop a transfer function for the neuron-spike response, or output ($V(s)$), to a particular
 201 spike input ($I(s)$). Using a transfer function for each neuron which is represented as a single compartment,
 202 we are able to efficiently associate the configuration of the filters with the structure of the neural network as
 203 well as the individual characteristics of each neuron. On top of that, we also are able to focus on frequency
 204 domain for an effective spike firing filtering. We rely on the electronic interpretation of the Hodgkin-Huxley
 205 model of neuron action potentials, which is made based on the neuronal cable theory assumptions on the
 206 static ionic channels conductance. In this section, we provide the details of the development of the transfer
 207 function, which is built on the linearization process of the Hodgkin-Huxley neuron model.

208 2.2.1 Hodgkin-Huxley Formalism

209 As aforementioned in Section 1, neurons can perform spike filtering tasks either by manipulating ionic
 210 conductances, such as sodium and potassium conductances, from within the cell (Fortune and Rose, 1997)
 211 or by working on the extracellular environment where the synapse occurs (Brunel et al., 2001; Moreno-Bote
 212 and Parga, 2004). Furthermore, filtering capabilities may vary according to the non-linearities of the
 213 neuron's activity and action potential propagation. In order to design an efficient filtering process, we will
 214 need to eliminate the non-linearities so we can directly link neurons properties to the filtering behavior
 215 and adjust these properties according to a desired filtering performance level. We consider the Hodgkin
 216 and Huxley non-linear model (Pospischil et al., 2008) as our basic model since it perfectly describes the
 217 influence of ionic conductance and synaptic conductance in the propagation of the action potentials. We
 218 assume that parts of the neuron will constitute a compartment, which results in the electric circuit in Fig. 3A
 219 when applying the conventional neural cable theory.

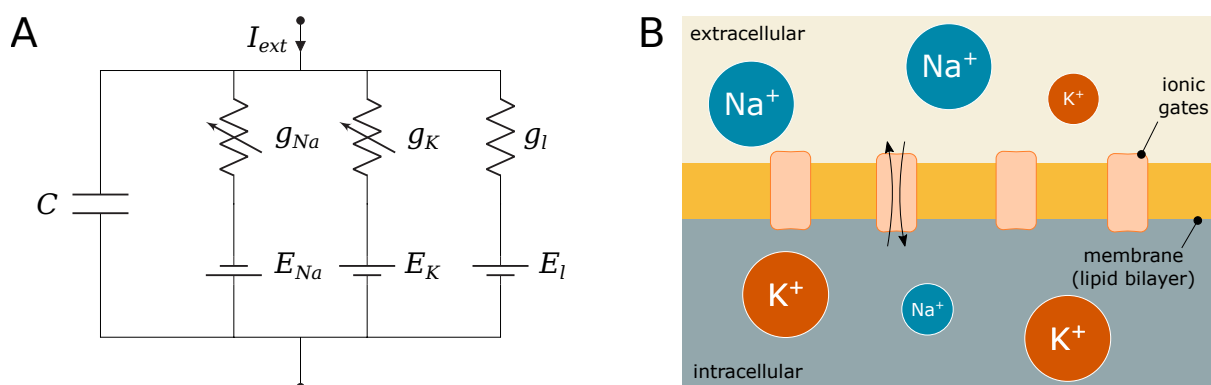


Figure 3. Hodgkin-Huxley (HH) model: (A) Electronic circuit representation and (B) Equivalent biological HH compartment; the lipid bilayer is modeled as C , the conductances g represent how open or close the ionic gates are and the gradient of ions between the intra- and extra-cellular space define the reversal potentials E .

220 Figure 3 depicts C as the membrane capacitance, each voltage-gated ionic channel represented by its
 221 respective conductances g_{Na} and g_K and the leak channel by the linear conductance g_l . The membrane
 222 capacitance is proportional to the surface area of the neuron and, along with its resistance, dictates how fast
 223 its potential responds to the ionic flow. The ratio between intra- and extra-cellular ions define the reversal
 224 potentials $E_{Na, K, l}$ establishing a gradient that will drive the flow of ions (Barreto and Cressman, 2011).

225 When an external stimulus, I_{ext} , is presented, it triggers either the activation or inactivation of the ionic
 226 channels that allow the exchange of ions that result in depolarization (or hyperpolarization when inhibitory)
 227 of the membrane of the cell. These dynamics are modeled as

$$C \frac{dV}{dt} = -I_l - I_{Na} - I_K + I_{ext}, \quad (1)$$

228 where V is the membrane potential and I_x are the ionic currents where x represents either a specific ion
 229 (Na , K) or the leak channel (l). Those currents are described as

$$I_l = g_l(V - E_l), \quad (2)$$

$$I_{Na} = g_{Na} m^3 h (V - E_{Na}), \quad (3)$$

$$I_K = g_K n^4 (V - E_K), \quad (4)$$

230 where m and h are the activation and inactivation variables of the sodium channel, respectively, and n is the
 231 activation variable of the potassium channel, following the conventional approach described by Hodgkin
 232 and Huxley (1952) and stated as

$$\frac{dm}{dt} = \alpha_m(V)(1 - m) - \beta_m(V)m, \quad (5)$$

$$\frac{dh}{dt} = \alpha_h(V)(1 - h) - \beta_h(V)h, \quad (6)$$

$$\frac{dn}{dt} = \alpha_n(V)(1 - n) - \beta_n(V)n, \quad (7)$$

233 in which the values of the rate constants α_i and β_i for the i -th ionic channel can be defined as

$$\alpha_m = \frac{0.1(V + 40)}{1 + e^{-(V+40)/10}}, \quad (8)$$

$$\beta_m = 4e^{-(V+65)/20}, \quad (9)$$

$$\alpha_h = 0.07e^{-(V+65)/20}, \quad (10)$$

$$\beta_h = \frac{1}{1 + e^{-(V+35)/10}}, \quad (11)$$

$$\alpha_n = \frac{0.01(V + 55)}{1 - e^{-(V+55)/10}}, \quad (12)$$

$$\beta_n = 0.125e^{-(V+65)/80}. \quad (13)$$

234 The membrane capacitance is proportional to the size of the cell, and on the other hand, the bigger
 235 the cell diameter, the lower the spontaneous firing rate (Sengupta et al., 2013). Furthermore, each ionic
 236 channel can be studied as containing one or more physical gates which can assume either a permissive or
 237 a non-permissive state when controlling the flow of ions. The channel is open when all gates are in the
 238 permissive state, and it is closed when all of them are in the non-permissive state (Baxter and Byrne, 2014).

239 2.2.2 Hodgkin-Huxley Linear Model

240 In order to derive a transfer function for the Hodgkin-Huxley model, we must consider each neuron as
 241 a system that is linear and time-invariant (LTI). If the system is non-linear, then a linearization process
 242 should be done before any frequency analysis is performed. For a more detailed analysis on the procedures
 243 for linearization of the Hodgkin-Huxley model, the reader is referred to (Koch, 2004; Mauro et al., 1970;
 244 Sabah and Leibovic, 1969; Chandler et al., 1962).

245 The linearization process requires that we reconsider the electronic components in each neuron
 246 compartment to adequately eliminate trivial relationships. Membranes with specific types of voltage-
 247 and time-dependent conductances can behave as if they had inductances even though neurobiology
 248 does not possess any coil-like elements. This modification will transform the behavior of non-linear
 249 components towards linearization, resulting in a proportional relationship between the voltage and current
 250 changes (Koch, 2004).

251 Every linearization process is performed for small variations around a fixed point, hereafter denominated
 252 by δ , and in the case of the Hodgkin-Huxley model, this fixed point should be the steady-state (resting
 253 state) of the system. Because the sodium activation generates a current component that flows in an opposite
 254 direction compared to that of a passive current, the branch concerning the sodium activation should
 255 have components with negative values while the branches regarding potassium activation and sodium
 256 inactivation should have components with positive values (Sabah and Leibovic, 1969). The linear version
 257 of the circuit of Figure 3A is illustrated in Figure 4, where C is the membrane capacitance, g_n , g_m and g_h
 258 are the conductances of the inductive branches connected in series with their respective inductances L_n ,
 259 L_m and L_h derived from the linearization process and $G_T = G_L + G_K + G_{Na}$ is the total pure membrane
 260 conductance.

261 Let us consider the membrane potential deviation, δV , around some fixed potential. Thus, we can express
 262 the response of the circuit to small-signal inputs as

$$C \frac{d\delta V}{dt} = I_{ext} - \delta I_l - \delta I_K - \delta I_{Na}, \quad (14)$$

263 where $\delta I_{l,Na,K}$ are current variations at any given steady-state and can be defined as

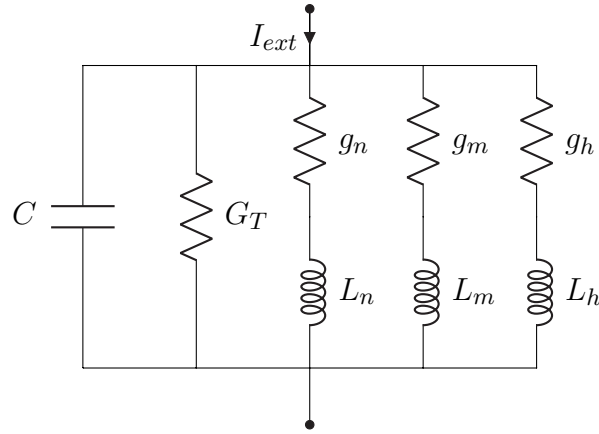


Figure 4. Hodgkin-Huxley linear circuit model representation.

$$\delta I_l = g_l \delta V, \quad (15)$$

$$\delta I_K = G_K \delta V + 4g_K n_\infty^3 (V - E_K) \delta n, \quad (16)$$

$$\delta I_{Na} = G_{Na} \delta V + 3g_{Na} m_\infty^2 h_\infty (V - E_{Na}) \delta m + g_{Na} m_\infty^3 (V - E_{Na}) \delta h, \quad (17)$$

264 where $G_{K,Na}$ are pure conductances of potassium and sodium and G_L the pure leak conductance expressed
265 as

$$G_L = \bar{g}_l, \quad (18)$$

$$G_K = \bar{g}_K n_\infty^4, \quad (19)$$

$$G_{Na} = \bar{g}_{Na} m_\infty^3 h_\infty, \quad (20)$$

266 where $\bar{g}_{K,Na}$ are the maximum attainable conductances, and δn , δm and δh are small variations around the
267 steady-state of the activation and inactivation variables n , m and h which are written as

$$\frac{d\delta n}{dt} = \frac{d\alpha_n}{dV} \delta V - (\alpha_n + \beta_n) \delta V - n_\infty \left(\frac{d\alpha_n}{dt} - \frac{d\beta_n}{dt} \right) \delta V, \quad (21)$$

$$\frac{d\delta m}{dt} = \frac{d\alpha_m}{dV} \delta V - (\alpha_m + \beta_m) \delta V - m_\infty \left(\frac{d\alpha_m}{dt} - \frac{d\beta_m}{dt} \right) \delta V, \quad (22)$$

$$\frac{d\delta h}{dt} = \frac{d\alpha_h}{dV} \delta V - (\alpha_h + \beta_h) \delta V - h_\infty \left(\frac{d\alpha_h}{dt} - \frac{d\beta_h}{dt} \right) \delta V, \quad (23)$$

268 as a function of the derivative of the rate constants $\alpha_{n,m,h}$ and $\beta_{n,m,h}$, and n_∞ , m_∞ and h_∞ are the
269 steady-state values of m , n and h defined as

$$n_\infty = \frac{\alpha_n}{\alpha_n + \beta_n}, \quad (24)$$

$$m_\infty = \frac{\alpha_m}{\alpha_m + \beta_m}, \quad (25)$$

$$h_\infty = \frac{\alpha_h}{\alpha_h + \beta_h}, \quad (26)$$

270 and the conductances, $g_{n,m,h}$, and inductances, $L_{n,m,h}$, of the inductive branches are defined as

$$g_n = \frac{4\bar{g}_K n_\infty^3 (V - E_K) \left[\left. \frac{d\alpha_n}{dV} \right|_r - n_\infty \left. \frac{d(\alpha_n + \beta_n)}{dV} \right|_r \right]}{\alpha_n + \beta_n}, \quad (27)$$

$$L_n = \frac{1}{g_n(\alpha_n + \beta_n)}, \quad (28)$$

$$g_m = \frac{3\bar{g}_{Na} m_\infty^2 h_\infty (V - E_{Na}) \left[\left. \frac{d\alpha_m}{dV} \right|_r - m_\infty \left. \frac{d(\alpha_m + \beta_m)}{dV} \right|_r \right]}{\alpha_m + \beta_m}, \quad (29)$$

$$L_m = \frac{1}{g_m(\alpha_m + \beta_m)}, \quad (30)$$

$$g_h = \frac{\bar{g}_{Na} m_\infty^3 (V - E_{Na}) \left[\left. \frac{d\alpha_h}{dV} \right|_r - h_\infty \left. \frac{d(\alpha_h + \beta_h)}{dV} \right|_r \right]}{\alpha_h + \beta_h}, \quad (31)$$



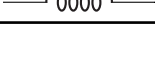
$$L_h = \frac{1}{g_h(\alpha_h + \beta_h)}. \quad (32)$$

271 Each channel has a probability of being open which represents the fraction of gates in that channel that
272 are in the permissive state (Gerstner et al., 2014). The gating variables are described by the coupling of
273 the conductances $g_{n,m,h}$ and their respective inductances $L_{n,m,h}$ which are functions of the rate constants
274 representing the transition from permissive to non-permissive state, $\alpha(V)$, and vice-versa, $\beta(V)$ which
275 should take a short period of time, $\tau = [\alpha(V) + \beta(V)]^{-1}$, to eventually reach a steady-state value, α_∞ and
276 β_∞ (Koslow and Subramaniam, 2005).

277 Borrowing concepts from systems theory such as frequency analysis of LTI systems, as a standard
278 procedure for the analysis of linear differential equations as simpler algebraic expressions, see (Nise, 2015),
279 and the linearization of non-linear systems for the reason previously mentioned at the beginning of this
280 section, we derived a transfer function in the *Laplace* domain for the linear system from Figure 4. The

281 relationship between the different elements of the circuit and their respective impedance and admittance
282 values from the *Laplace* transforms are depicted in Table 1.

Table 1. Impedance relationships for capacitors, resistors and inductors.

Component	Impedance	Admittance
Capacitor 	$\frac{1}{Cs}$	Cs
Resistor 	R	$G = \frac{1}{R}$
Inductor 	Ls	$\frac{1}{Ls}$

283 Therefore, the relationship between the output and the input of the system in the frequency domain is
284 expressed as

$$\frac{V(s)}{I(s)} = \frac{s^3 L_n L_m L_h}{\{L_n L_m L_h [s^4 C + s^3 (G_T + g_n + g_m + g_h)] + s^2 (L_m L_h + L_n L_h + L_m L_h)\}} \quad (33)$$

285 where $s = \sigma + j\omega$ is a complex variable; $j = \sqrt{-1}$ and $\omega = 2\pi f$, where f is the frequency in Hertz. Let
286 us rewrite Eq. (33) as

$$W(s) = C^{-1} \frac{s}{s^2 + sC^{-1}(G_T + g_n + g_m + g_h) + C^{-1}(L_m^{-1} + L_n^{-1} + L_h^{-1})}. \quad (34)$$

287 Now, denoting $\gamma = G_T + g_n + g_m + g_h$ and $\lambda^{-1} = L_n^{-1} + L_m^{-1} + L_h^{-1}$ and performing a few algebraic
288 manipulations, we end up with the following transfer function for the filter model

$$W(s) = \gamma^{-1} \frac{C^{-1}\gamma s}{s^2 + C^{-1}\gamma s + \lambda^{-1}C^{-1}}. \quad (35)$$

289 For frequency response analysis, we observe the behaviour of $W(j\omega)$, i.e. substitute $s = j\omega$. For $\omega \rightarrow 0$,
290 $W(j\omega)$ behaves like ω ; for $\omega \rightarrow \infty$ it behaves like $\frac{1}{\omega+1}$, i.e. in both cases it tends to zero, and hence
291 demonstrates the behaviour of a second-order band-pass filter (BPF). It corresponds to the canonical form
292 $\frac{K(\omega_0/Q)s}{s^2 + (\omega_0/Q)s + \omega_0^2}$ where $K = \gamma^{-1}$ is the gain, $Q = \gamma^{-1}\sqrt{C\lambda^{-1}}$ is the selectivity and $\omega_0 = \sqrt{\lambda^{-1}C^{-1}}$ is
293 the peak frequency of the filter. This agrees with findings from previous literature on the matter (Plesser
294 and Geisel, 1999) that concluded the periodicity of a stimulus is optimally encoded by a neuron only in a
295 specific spectral window.

296 2.3 Transfer Function Filter Design

297 Given the transfer function for a neural compartment in the previous section, we now progress towards
298 a transfer function for the spike filter. The filter is comprised of neurons that are particularly chosen to
299 have a network that will behave as a digital gate and a small population that will behave as a circuit that

300 implements the filter. Our aim is to capture the relationship between compartments as well as neuron
 301 connections so we can build a transfer function for the filter while considering neuron connection variables
 302 (synaptic conductance and synaptic weight) that allow easy reconfiguration of the filtering process. The
 303 linearization process combined with the analysis of the neuron communications is the driver of the filtering
 304 process, which also allows the derivation of a filter transfer function which is detailed below.

305 2.3.1 Biological Logic Gates and Circuits

306 Synthetic biology is the technology that allows the control of the neurons' internal process in order to
 307 construct non-natural activity and functioning of neurons, e.g. logic gates (Larouche and Aguilar, 2018).
 308 Synthetic logic operations inspire scientists to address the challenges posed by novel synthetic biomedical
 309 systems, such as biocompatibility and long-term use.

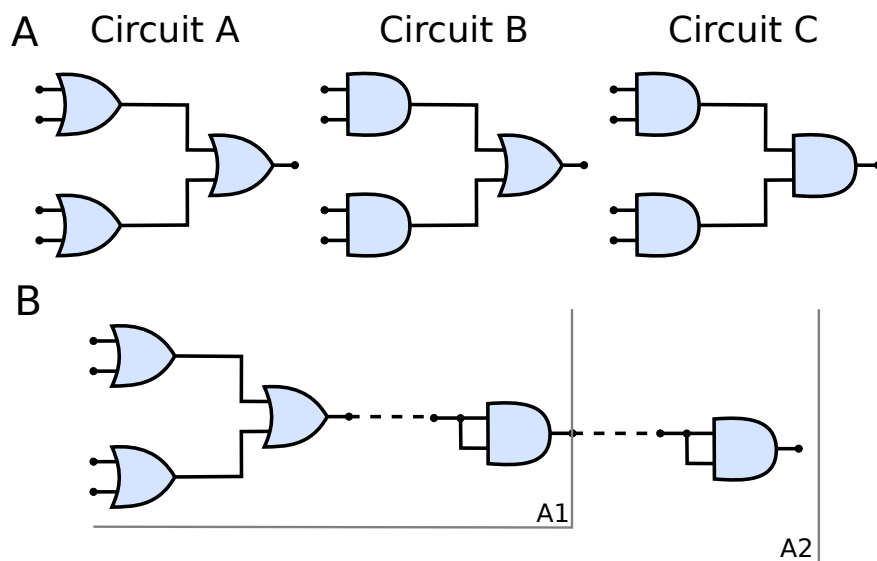


Figure 5. (A) Schematic of circuits A, B and C and (B) The connection of AND gates in cascade to circuit A. A1 refers to the arrangement described by a single AND gate connected to the output of the circuit A and A2 refers to another AND gate connected to the output of A1 arrangement, i.e. two AND gates in cascade with circuit A. Analogous nomenclature is employed for both circuits B, as in B1/B2 and C, as in C1/C2.

310 Figure 5A shows the three types of the circuit we have built and analyzed in this work. From circuits A to
 311 C, the number of OR gates is decreased; when compared to AND gates, OR gates are quite permissive. In
 312 our previous study

313 Given that several factors such as connection probability, type of cell, and different numbers of
 314 compartments (as discussed in Section 2.3.2) among different types of neurons may influence its gating
 315 capabilities. This variation on the quantity of compartments could also lead to variations on periods for
 316 the action potential to reach the post-synaptic terminals and start the synapse process. Furthermore, cells
 317 with bigger sizes of soma may take more time and amount of stimuli to reach threshold for action potential
 318 initiation (Sengupta et al., 2013), thus, also affecting the way a neuronal logic gate would work regarding
 319 a specific morphological neuronal type. For that reason, it is safe to keep two cells fixed as inputs (as
 320 illustrated in Figure 1) and then deploy an arrangement with which its performance has been previously
 321 assessed, allowing us to be fairly certain about how the synthetic gate or circuit should behave. Each neuron

322 is represented by a block, $W_i(s)$ for the i -th neuron, and its representation in the frequency domain is
 323 proposed in Equation (35) and further detailed in Subsection 2.3.2.

324 2.3.2 Compartmental Modelling

325 Neurons are very complex structures with numerous ramifications and several factors that contribute
 326 to their highly non-linear dynamism. Aiming to make the comprehension of such a complex electrical
 327 behavior easier, one employs a widely used technique called “compartmental modelling”. Since different
 328 neurons have different morphologies, the mechanism of determining the number of compartments will
 329 be based on estimating the length of a specific neuronal structure. For instance, a varying length of axon,
 330 which will reflect in different quantities of compartment in series, where we will have a fixed size for
 331 each segment of the axon representing one compartment. This is a very natural and elegant way to model
 332 dynamic systems as multiple interconnected compartments where each compartment is described by its
 333 own set of equations, carrying the influence of one compartment to the next reproducing the behavior of
 334 the whole neuron.

335 Observing the neuron as a set of compartments described by transfer functions equivalent to that of (35),
 336 the neuronal morphology of a pyramidal cell, as illustrated in Figure 6A, (or any cell for that matter) can
 337 be modeled as an electrical circuit as shown in the topology of Figure 6B; the dendritic ramifications are
 338 modeled as a combination of serial and parallel connections terminanting in the soma which is connected to
 339 the axon modeled as a series of compartments; its interpretation in terms of filtering is given in Figure 6C.
 340 The effect of a serial connection of two compartments is one of set-intersection when observed in the
 341 frequency domain: two bandpass filters in series pass only the frequencies that exist in both of their
 342 passbands. On the other hand, a parallel connection has a set-union effect, a parallel connection of filters
 343 will pass all the frequencies in both their passbands. As such, a large network (tree) of such compartments
 344 with similar bands combined in a cell, and cells combined in a group of cells will exhibit asymptotic
 345 bandpass behavior as well.

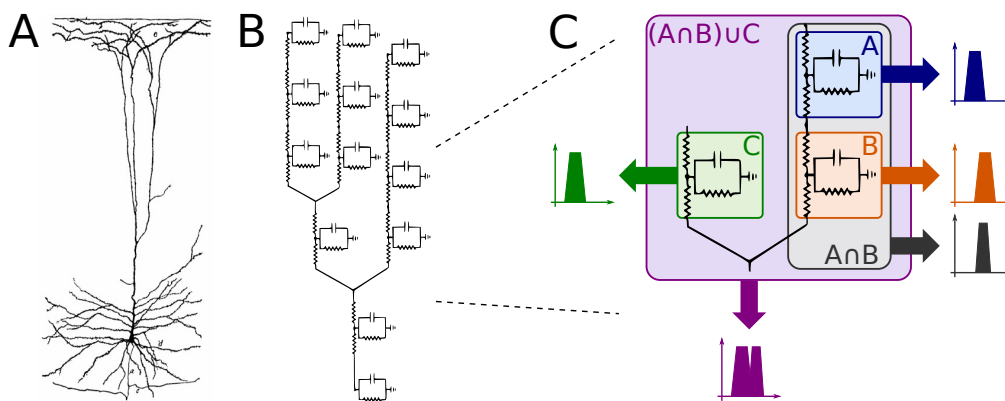


Figure 6. Compartmental neuron representation: (A) Natural topology of a pyramidal cell, (B) Electronic circuit compartments and (C) Effects of serial and parallel connections between compartments.

346 Every single compartment, each represented by one transfer function, is grouped in trees of three cells
 347 (Figure 1) forming a logic gate; the three gates are connected into a tree of their own, as illustrated in
 348 Figure 5A, forming a logic circuit. All of the cells are represented with the same form of the transfer
 349 function,

$$W_i(s) = \zeta_i \gamma_i^{-1} \frac{C_i^{-1} \gamma_i s}{s^2 + C_i^{-1} \gamma_i s + \lambda_i^{-1} C_i^{-1}}, \quad i = 1, \dots, 9 \quad (36)$$

350 with symbols defined previously, and a new parameter ζ_i describing the synaptic weight for the i th cell; ζ_i
351 acts as a tunable gain for the neurons.

352 Using the parameters from (Mauro et al., 1970) aiming to keep them within the physically sensible orders
353 of magnitude, we obtain the reference values of $\bar{\gamma} = 0.0024$, $\bar{\lambda} = 119$, $\bar{C} = 1$ and $\bar{\zeta} = 1$, and the values
354 for 9 cells were generated multiplying these reference values by a uniformly distributed random variable
355 in the range $(0, 1)$. This kind of distribution is widely used to describe experiments where an arbitrary
356 result should lie between certain boundaries, and in our case boundaries are defined by reasonable orders
357 of magnitude around values made available by previous studies; keeping exactly the same parameters for
358 all cells in the cascade is not realistic. The total transfer function of this system is

$$W = ((W_1 + W_2)W_3W_7 + (W_4 + W_5)W_6W_8)W_9, \quad (37)$$

359 and its frequency response (Bode plot) for the relevant range of frequencies in our applications (Wilson
360 et al., 2004) is shown in Figure 7B.

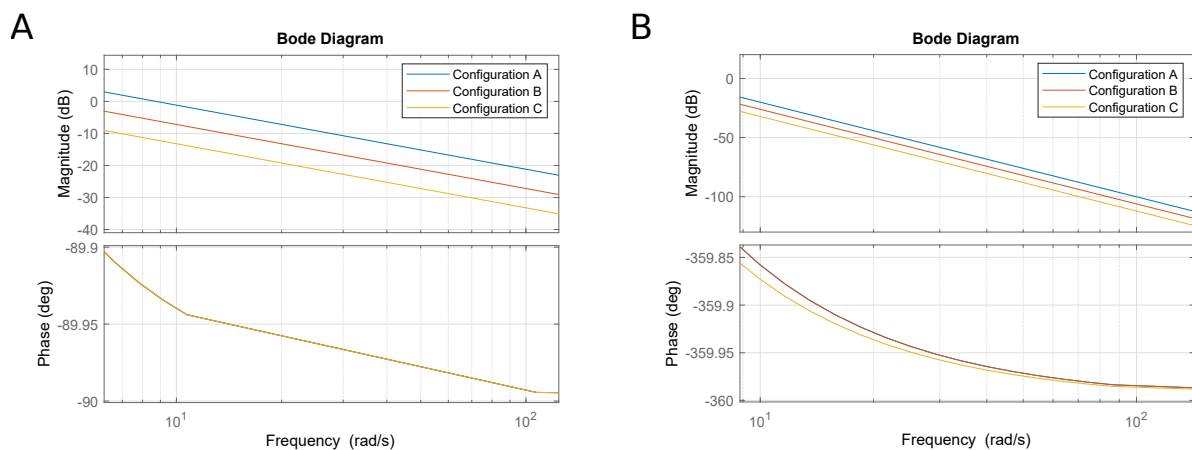


Figure 7. Bode plots: (A) Single second-order bandpass filter approximation and (B) Filter structure from Eq. (37)

361 Let us now observe three cases concerning the choice of ζ_i values. In the first case, we keep all of them
362 at unity and consider it our base case for this part of the analysis (and to keep it aligned with the rest of
363 the paper, we call it *Circuit B*). In the second case, we double the values of ζ_3 and ζ_6 , which corresponds
364 to the manipulation of the output cell for the two input gates in *Circuit A*. In our linear model, this is
365 equivalent to doubling ζ_9 and leaving everything else intact. Finally, in the third case, we manipulate the
366 output cell of the last gate by halving its synaptic conductance (*Circuit C*). This effectively means that the
367 three cases are $\zeta_{9B} = 1$, $\zeta_{9A} = 2$ and $\zeta_{9C} = 1/2$, respectively. Since the tunable gain ζ_9 of the gate W_9 , is
368 the tunable gain of the whole system W according to (37), its change would offset the frequency response
369 along the ordinate axis, i.e. lower gains (lower conductance) would suppress the unwanted frequencies in a
370 better way, while higher gains would do the opposite. This is demonstrated in Figure 7A. The process of

371 the analysis is summarized in Algorithm 1 and a summary with all elements from both the original and
 372 linearized versions of the Hodgkin-Huxley as well as the transfer function model is presented in Table 2.

1 Initialize:

2 $\Gamma = \{\gamma_1, \dots, \gamma_9\} \in (0, \bar{\gamma})$

3 $\Lambda = \{\lambda_1, \dots, \lambda_9\} \in (0, \bar{\lambda})$

4 $\mathcal{C} = \{C_1, \dots, C_9\} \in (0, \bar{C})$

5 $Z = \{\zeta_1, \dots, \zeta_9\} \in (0, \bar{\zeta})$

6 **for** $1 \leq i \leq 9$ **do**

7 $W_i \leftarrow \zeta_i \gamma_i^{-1} \frac{C_i^{-1} \gamma_i s}{s^2 + C_i^{-1} \gamma_i s + \lambda_i^{-1} C_i^{-1}}$

8 **end**

9 $W_B \leftarrow ((W_1 + W_2)W_3W_7 + (W_4 + W_5)W_6W_8)W_9$

10 $W_A \leftarrow 2W_B$

11 $W_C \leftarrow 0.5W_B$

12 Plot frequency response: W_A, W_B, W_C

Algorithm 1: Linear model filter analysis

373 Alternatively, as we suggested earlier, a single transfer function of a compartment serves as an
 374 approximation of the entire system due to the effects of repeated bandpass filtering in Figure 6C. In
 375 such case, we observe 20 dB/decade slope in the Bode plot shown in Figure 7A (as compared to 80
 376 dB/decade slope in Figure 7B) and the same offset of $20 \cdot \log_{10} 2 \approx 6$ dB in case of halving/doubling the
 377 synaptic weight. Since the filter is of a band-passing nature, it is only natural that, around the resonant
 378 frequency, lower and higher frequency amplitudes should be ideally attenuated towards zero. Thus, it is
 379 worth mentioning that in both cases depicted here, the part of the frequency response with the cusp is at
 380 very low frequencies, so it is not visible in the relevant part of the spectrum. As such, the filter behaves as a
 381 low pass filter for all practical considerations.

3 RESULTS

382 In this section, we discuss the simulation results concerning the reconfigurable logic gates as well as the
 383 circuits. For all simulations, intrinsic parameters of the cell were kept at their default values (such as the
 384 length and diameter of each of their compartments) meaning that nothing concerning their morphological
 385 properties was changed, the spike trains fed to the input of the circuits followed a *Poisson* process and
 386 the threshold for spike detection and data analysis was 0 mV where any potential higher than that in a
 387 specific time slot would be considered a bit “1”, characterizing the use of a simple *On-Off Keying (OOK)*
 388 modulation which was implemented where a spike is considered as a bit ‘1’ and its absence a bit ‘0’ in each
 389 time slot. The cell models and information on their respective connection probabilities between different
 390 pair of neurons were obtained from the work of Markram et al. (2015), and then we used NEURON and
 391 Python for simulation and data analysis (Carnevale and Hines, 2009; Hines et al., 2009). The source-code
 392 of our simulations is publicly available on a GitHub repository¹.

393 3.1 Reconfigurable Logic Gates

394 In this work, we call “reconfigurable” logic gates, the gates that work by changing the synaptic weight
 395 between the connections of both input cells with the output cell in a neuronal logic gate structure. Aiming

¹ <https://github.com/gladonias/neuronal-filters>

Table 2. Summary of elements described in the proposed model.

Element	Description
C	Membrane capacitance
g_{Na}, g_K, g_l	Sodium, potassium and leak conductances
E_{Na}, E_K, E_l	Sodium, potassium and leak reversal potentials
I_{ext}	External stimulus
I_{Na}, I_K, I_l	Ionic current for the sodium, potassium and leak channels
V	Membrane potential
m, h	Sodium activation and inactivation variables
n	Potassium activation variable
α, β	Rate constants for m, h and n from permissive to non-permissive state and vice-versa
δ	Small variation around the steady-state
G_T	Total pure conductance
G_{Na}, G_K, G_L	Sodium, potassium and leak pure conductances
$\bar{g}_{Na}, \bar{g}_K, \bar{g}_l$	Maximum attainable sodium, potassium and leak conductances
$m_\infty, h_\infty, n_\infty$	Steady-state values of m, h and n
g_m, g_h, g_n	Conductances of the inductive branches
L_m, L_h, L_n	Inductances of the ionic paths
W	Transfer function of the filter
K, Q, ω_0	Gain, selectivity and peak frequency of the filter
ζ	Synaptic weight

396 to measure individual gate accuracy, the spike trains in the inputs were randomly produced but we control
 397 their frequency variation, in other words, for each simulation, the frequency at all inputs was the same and
 398 any change in the frequency was performed for all inputs of the gates meaning that none of the simulations
 399 account for different frequency values between different inputs in a single simulation. The accuracy is
 400 a simple but powerful measure for the performance of the gates, with which we intend to analyze the
 401 effects of the dynamics of the cell on the output of the circuit when comparing this output with the ideal
 402 response of the circuit derived from its truth-table. The accuracy is calculated according to the following
 403 equation (Hanisch and Pierobon, 2017):

$$A(E[Y]; Y) = \frac{P_{1,1} + P_{0,0}}{\sum_Y \sum_{E[Y]} P_{Y,E[Y]}}, \quad (38)$$

404 where $P_{Y,E[Y]}$ is the probability of Y given $E[Y]$ in which Y is the actual output and $E[Y]$ is the expected
 405 output and $Y \& E[Y] \in \{0, 1\}$. $P_{Y,E[Y]}$ resembles the conditional probabilities in a binary symmetric
 406 channel (BSC). Thus, $P_{0,0} = 1 - P_{1,0}$, and $P_{0,1} = 1 - P_{1,1}$. It is possible to calculate $P_{1,1}$, for instance,
 407 by counting the number of bits there are for each input-output combination. In other words, considering
 408 $\#B_{i,j}$ the number of times a bit i was received when bit j was sent knowing that $i \& j \in \{0, 1\}$, then
 409 $P_{1,1} = \#B_{1,1} / (\#B_{1,1} + \#B_{0,1})$.

410 Given the objective of obtaining a behavior similar to an OR gate, the synaptic weight should be set to
 411 $0.06 \mu\text{S}$, meaning that the pre-synaptic stimuli will drive a higher influence on the depolarization of the
 412 post-synaptic cell. On the other hand, for an AND behavior, the weight is set to $0.03 \mu\text{S}$, which reduces the

413 influence of a single spike and look to a response of the post-synaptic neuron only when two spikes arrive
 414 very close to each other in terms of time. This is conducted so we have acceptable levels of accuracy when
 415 compared to the expected outputs of the gate.

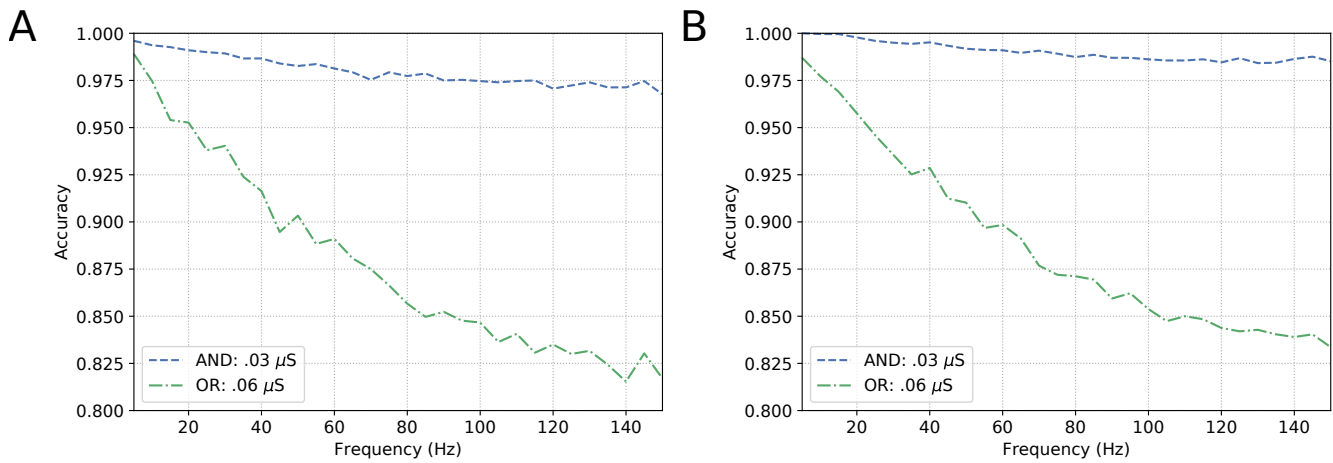


Figure 8. Analysis on reconfigurable logic gates with neurons of types (A) L23-MC, L23-NBC and L1-DAC and (B) L23-MC, L23-NBC and L1-HAC.

416 Figures 8 show similar responses when gates originally built to be of a specific kind. This means either
 417 OR or AND gates can change their configurations that drives their gating capabilities by modifying the
 418 synaptic weight between the connections of the input cells and the output cell. Although there is quite a
 419 visible difference between the performance of AND and OR gates, even at high frequencies (150 Hz), the
 420 accuracy of the reconfigurable logic gates remains above 80%.

421 3.2 Neuronal Logic Circuits

422 Once the reconfigurable behavior of the gates is assessed, they are connected to other gates to form a
 423 logic circuit. The performance is measured employing a ratio (frequency response), i.e. the number of
 424 spikes (bits '1') in the output divided by the nominal input frequency, in Hertz. This ratio is also known as
 425 the magnitude, or gain when evaluating the data in decibels. Following the approach for individual gates,
 426 the inputs are random and the frequency is increased uniformly. Since the gates showed similar accuracy
 427 when increasing the input frequency, we picked the one analyzed in Figure 8A for our circuit analysis with
 428 a reconfigurable logic gate, modifying only the output gate's synaptic properties.

429 Figures 9A show the results for the circuits in Figure 5A. As expected, Circuit C has a stronger attenuation
 430 of the signals passing through it, and this is mainly due to the fact it is an arrangement with three AND
 431 gates and, based on the truth table, an AND gate only responds to stimuli if all its inputs are active at the
 432 same time. The magnitude in decibels shown in Figure 9B follow a standard presentation of the response
 433 of digital filters.

434 In the non-linear case of the system, the filtering is even better than what the linear model would promise,
 435 i.e. the suppression of unwanted frequencies is better due to superexponential decay. Let us compare
 436 Figure 7B and Figure 9B. The linear model suggests that a constant difference of 6 dB is to be expected
 437 if the synaptic weight of the output cell is halved (or doubled), and a linear, constant amplitude drop. In
 438 the nonlinear model, we do observe a 20 dB/decade drop and 6 dB difference at relevant frequencies, but
 439 instead of a linear trend, we observe a convex response, which helps in attenuating high frequencies faster

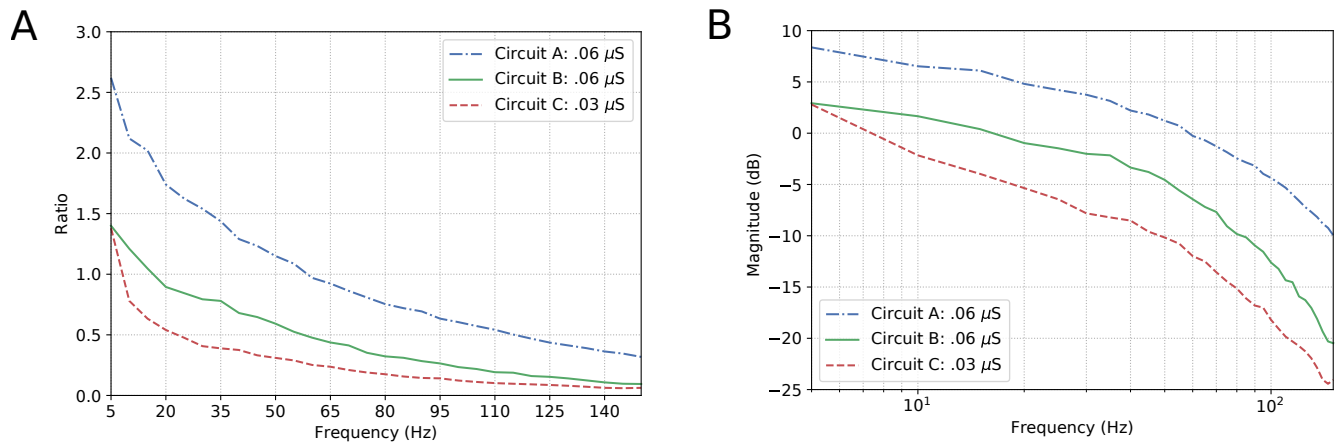


Figure 9. Effects of dynamic changes to the synaptic weight in circuits A, B and C; (A) Frequency response and (B) Magnitude in decibels.

440 than we would expect from the linear model. This is because the linear model is accurate in a neighborhood
 441 of the point at which it was linearized.

442 Now, let us consider $H(\nu)$ as the response of an ideal low-pass filter, and $W(\nu)$ the response of the
 443 proposed neuronal filter, the counter-efficiency of W given H is calculated as

$$\psi(W|H) = \int_0^{\nu_c} |W(\nu) - H(\nu)| d\nu + \int_{\nu_c}^{\nu_f} |W(\nu)| d\nu \quad (39)$$

444 where ν_c is the cut-off frequency and ν_f is the last evaluated frequency (in this relationship, the lower the
 445 value, the more efficient the filter is). Since, in terms of magnitude, a frequency band when cut by an ideal
 446 filter should be attenuated towards negative infinity ($-\infty$), we have to pick a limit for the calculation of the
 447 area under the curves. In our case, after a visual inspection, the baseline for calculation chosen was -25
 448 dB, because this is the closest integer value to the lowest values of magnitude.

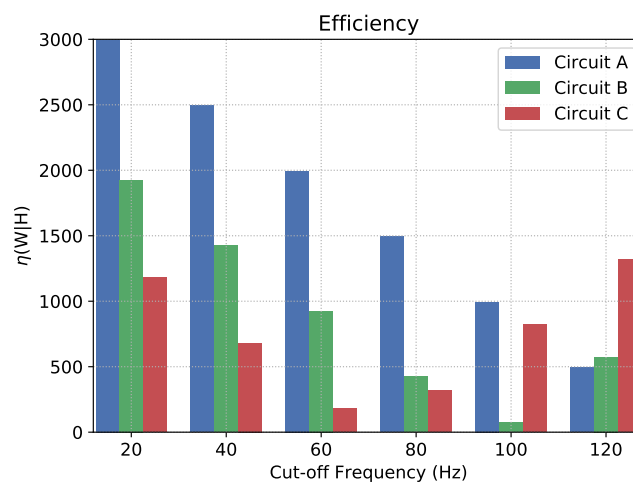


Figure 10. Counter-efficiency of the circuits when compared to ideal filters (the lower the value, the better the filter's performance).

449 Figure 10 depicts the counter-efficiency analysis performed for the three circuits. As it is shown, for
 450 different frequency bands we have some circuits performing better than others. Also, each circuit has a
 451 preferable frequency band for achieving maximum efficiency. For frequencies lower than or equal to 80 Hz,
 452 Circuit C seems the most efficient, especially at 60 Hz, while frequencies around 100 Hz show Circuit B as
 453 the most efficient which is also the band where it performs the best. Circuit A, on the other hand, has its
 454 best performance for 120 Hz, and probably for higher frequencies as well if the trend continues.

455 This shift in performance may allow us to control which type of circuit we want to activate inside the
 456 brain depending on which activity the subject is performing at the time, e.g. being awake or being asleep.
 457 These changes may be induced by the intake of specific drugs that alter synaptic properties in a neuronal
 458 connection.

459 Figure 11 shows a parallel analysis between the magnitude in dB and the accuracy of the filters with
 460 AND gates in cascade. Each circuit is identified by a pair of characters, the first is the letter referring to the
 461 circuit analyzed, the second is how many AND gates were connected in cascade. For example, A2 means
 462 Circuit A with two AND gates in cascade, as illustrated in Figure 5B.

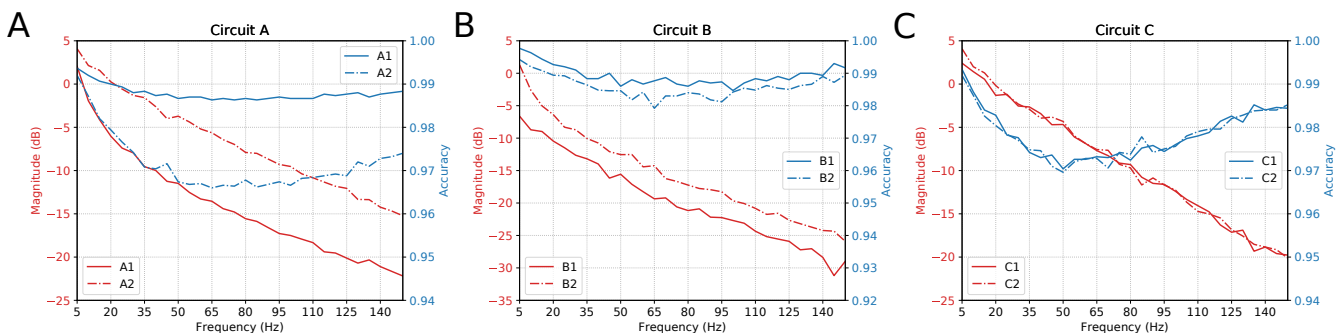


Figure 11. Parallel between Magnitude (dB) and Accuracy of the circuits with AND gates in cascade.

463 The results suggest that, by increasing the number of gates in cascade, we have to deal with attenuation
 464 in the network due to propagation caused by specific characteristics of the cell, such as the connection
 465 probability; hence, the more gates in cascade the worse the performance of the circuit. Also, even though
 466 the ratio keeps going downwards, at some point, the accuracy will start to shoot up. With careful evaluation,
 467 the dip in the accuracy along mid-range frequencies is very low in terms of scale, showing a difference of
 468 only around 0.03 on the values of accuracy.

4 DISCUSSION

469 Synaptic weight plays a role in the influence of the pre-synaptic stimuli and its impact on the post-synaptic
 470 neuron and has a value proportional to the synaptic conductance (Gardner, 1989) which is driven by the
 471 amount and type of neurotransmitters that are being bound to the post-synaptic terminals. The higher
 472 the connection probability between pairs of neurons, the stronger the influence of a specific synaptic
 473 weight. This is due to the proportional relationship that the weight has with each synaptic connection that
 474 individually releases a certain amount of neurotransmitters, hence, different neuron types may affect the
 475 influence of a fixed value of synaptic weight. This explains how the accuracy values fluctuate between
 476 different types of gates and circuits as shown in Fig. 11. Within a larger network spatial dimension, the

477 types of neurons may drive a higher accuracy fluctuation since the network connection exhibits different
478 synaptic weights between each other.

479 With our model, we have mainly investigated the attenuation on the spiking frequency for three different
480 types of circuits in which we decrease the number of OR gates by replacing them with AND gates.
481 We were also able to have the fine-tuning synaptic properties showing a difference of around 5 dB in
482 performance between the curves in Figure 9B. Changes in the synapse are also considered (Vogels and
483 Abbott, 2005), either by strengthening or weakening specific synaptic connections, logic gates were
484 built within a homogeneous network of integrate-and-fire neurons. Moreover, the experiments conducted
485 by (Goldental et al., 2014) followed a procedure that enforced stimulations on neuronal circuits within
486 a network of cortical cells *in-vitro* and they do propose other types of gates such as XOR and NOT.
487 Furthermore, we increased the number of AND gates in a cascade-like manner in order to confirm that
488 the longer the line of cascade gates, the more attenuated the signal should be if none of those elements
489 receives any kind of external stimuli despite the spike coming from the circuit, and this result is depicted
490 in Figure 11. A peak value in the difference of around 8 dB occurs in Circuit A, decreasing to around
491 5 dB in Circuit B and there is a small difference in Circuit C. The transfer function derived from the
492 Hodgkin-Huxley linear model suggests a band-pass behavior of the system (Plesser and Geisel, 1999) for
493 very low frequencies leaving us with a low-pass filter acting on higher frequencies ranging from 5 to 150
494 Hz. Considering the time for a spike to be fired that comprises depolarization, repolarization, and refractory
495 period, higher frequencies will lead to saturation and non-realistic behavior of neuronal firing.

496 Our results, therefore, suggest that neuronal logic circuits can be used to construct also digital filters,
497 filtering abnormal high-frequency activity which can have many sources including neurodegenerative
498 diseases. A metric of counter-efficiency was also proposed, which should show how far apart the real results
499 are from the ideal cases. We found that frequency bands were found to be of optimal value for different
500 types of circuits such as 60 Hz for circuit C, 100 Hz for circuit B, and 120 Hz for circuit A, as shown
501 in Figure 10. Based on the presented results, we demonstrate that by reconfiguring the gates inside the
502 digital filters we can shift the intensity with how we attenuate the spiking frequency allowing an on-the-fly
503 adaptation of the filtering tasks depending on the activity that is being performed by the subject where, for
504 instance, circuit C should outperform both A and B for frequencies lower than or equal to 80 Hz.

505 The envisioned application of the proposed mathematical framework is for *in-silico* pharmacology and
506 how it can be used to provide advanced prediction supporting computational strategies to test drugs. Since
507 drug design and discovery in neuroscience are very challenging, especially due to the complexity of
508 the brain and the significant impediment of the blood-brain barrier (BBB) imposes on the delivery of
509 therapeutic agents to the brain. The success rate for approval by competent authorities of such drugs is less
510 than 10%. Such a low rate is attributed not only to factors related to the disease itself, such as complexity,
511 slow development, and gradual onset but also, to the limited availability of animal models with good
512 predictive validity and the limited understanding of the biological side of the brain (Geerts et al., 2020).
513 The system model derived from a set of coupled neuron compartments can help push forward the design of
514 these neuronal filters and provide a platform for *in silico* drug-induced treatments on top of engineered
515 biological models of neurons. A platform that could lead to cost-effective drug development and analysis of
516 potential bio-computational units capable of enhancing signal processing in the brain, as well as predicting
517 long-term effects of using a specific drug are potential uses of the proposed mathematical framework.

5 CONCLUSION

518 In this work, we proposed a reconfigurable spike filtering design using neuronal networks that behave as a
519 digital logic circuit. This approach requires the cells to be sensitive to modifications through chemicals
520 delivered through several proposed methods available in the literature. From the Hodgkin-Huxley action
521 potential model we developed a mathematical framework to obtain the transfer function of the filter. This
522 required a linearization of the Hodgkin-Huxley model that changes the cable theory simplification for each
523 cell compartment. To evaluate the system, we have used our transfer function as well as the NEURON
524 simulator to show how the frequency of operation, logic circuit configuration as well as logic circuit
525 size can affect the accuracy and efficiency of the signal propagation. We observed that all-ANDs circuit
526 produces more accurate results concerning their truth-table when compared to all-ORs. In addition, the
527 results show that each digital logic circuit is also reconfigurable in terms of cut-off frequency of the filter,
528 by manipulating the types of gates in the last layer of the circuit.

529 We believe the proposed filter design and its mathematical framework will contribute to synthetic biology
530 approaches for neurodegenerative disorders such as epilepsy, by showing how the control of cellular
531 communication inside a small population can affect the propagation of signals. For future work, we plan
532 the use of non-neuronal cells, e.g. astrocytes, for the control of gating operations and the assessment of
533 neuronal filtering capabilities at a network level. Treatment techniques based on this method can be a
534 radical new approach to reaching precision and adaptable outcomes, inspired from electronic engineering
535 as well as communication engineering. Such techniques could tackle at a single-cell level, neurons affected
536 by seizure-induced high-frequency firing or bypass neurons that have been affected by a disease-induced
537 neuronal death and degeneration, thus keeping the neuronal pathway working at a performance as optimal
538 as possible.

CONFLICT OF INTEREST STATEMENT

539 The authors declare that the research was conducted in the absence of any commercial or financial
540 relationships that could be construed as a potential conflict of interest.

AUTHOR CONTRIBUTIONS

541 GA performed the simulations and wrote the first draft of the manuscript. HS performed the control-
542 theoretic analysis. GA, HS and MB performed the data analysis. SB, NM, MB and MW led the work
543 development. All authors contributed to manuscript writing and revision. All authors also have read and
544 approved the submitted version.

FUNDING

545 This publication has emanated from research conducted with the financial support of Science Foundation
546 Ireland (SFI) and is co-funded under the European Regional Development Fund for the CONNECT
547 Research Centre (13/RC/2077) and the FutureNeuro Research Centre (16/RC/3948).

REFERENCES

548 Adonias, G. L., Yastrebova, A., Barros, M. T., Balasubramaniam, S., and Koucheryavy, Y. (2019). A
549 Logic Gate Model based on Neuronal Molecular Communication Engineering. In *Proceedings of the*
550 *4th Workshop on Molecular Communications* (Linz, Austria), 15–16

- 551 Adonias, G. L., Yastrebova, A., Barros, M. T., Koucheryavy, Y., Cleary, F., and Balasubramaniam, S.
552 (2020). Utilizing Neurons for Digital Logic Circuits: A Molecular Communications Analysis. *IEEE*
553 *Transactions on NanoBioscience* 19, 224 – 236. doi:10.1109/TNB.2020.2975942
- 554 Balevi, E. and Akan, O. B. (2013). A Physical Channel Model for Nanoscale Neuro-Spike Communications.
555 *IEEE Transactions on Communications* 61, 1178–1187. doi:10.1109/TCOMM.2012.010213.110093
- 556 Barreto, E. and Cressman, J. R. (2011). Ion concentration dynamics as a mechanism for neuronal bursting.
557 *Journal of Biological Physics* 37, 361–373. doi:10.1007/s10867-010-9212-6
- 558 Baxter, D. A. and Byrne, J. H. (2014). Dynamical Properties of Excitable Membranes. In *From Molecules*
559 *to Networks*, eds. J. H. Byrne, R. Heidelberger, and M. N. Waxham (Boston: Academic Press), chap. 14.
560 3rd edn., 409 – 442. doi:https://doi.org/10.1016/B978-0-12-397179-1.00014-2
- 561 Bennewitz, M. F. and Saltzman, W. M. (2009). Nanotechnology for Delivery of Drugs to the Brain for
562 Epilepsy. *Neurotherapeutics* 6, 323 – 336. doi:https://doi.org/10.1016/j.nurt.2009.01.018. Nontraditional
563 Epilepsy Treatment Approaches
- 564 Blier, P. and De Montigny, C. (1987). Modification of 5-HT neuron properties by sustained administration
565 of the 5-HT1A agonist gepirone: Electrophysiological studies in the rat brain. *Synapse* 1, 470–480.
566 doi:10.1002/syn.890010511
- 567 Brunel, N., Chance, F. S., Fourcaud, N., and Abbott, L. F. (2001). Effects of Synaptic Noise and Filtering on
568 the Frequency Response of Spiking Neurons. *Phys. Rev. Lett.* 86, 2186–2189. doi:10.1103/PhysRevLett.
569 86.2186
- 570 Carnevale, N. T. and Hines, M. L. (2009). *The NEURON Book* (New York, NY, USA: Cambridge University
571 Press), 1st edn.
- 572 Chandler, W., Fitzhugh, R., and Cole, K. S. (1962). Theoretical Stability Properties of a Space-Clamped
573 Axon. *Biophysical Journal* 2, 105 – 127. doi:https://doi.org/10.1016/S0006-3495(62)86844-1
- 574 Chaubey, S. and Goodwin, S. J. (2016). A Unified Frequency Domain Model to Study the Effect
575 of Demyelination on Axonal Conduction. *Biomedical Engineering and Computational Biology* 7,
576 BECB.S38554. doi:10.4137/BECB.S38554
- 577 Feng, T., Huang, X., Ni, R., Suen, W. L. L., and Chau, Y. (2019). Nanoparticles for drug delivery targeting
578 neurodegeneration in brain and eye. In *Nanomaterials for Drug Delivery and Therapy*, ed. A. M.
579 Grumezescu (William Andrew Publishing). 149 – 183. doi:https://doi.org/10.1016/B978-0-12-816505-8.
580 00006-0
- 581 Fortune, E. S. and Rose, G. J. (1997). Passive and Active Membrane Properties Contribute to the
582 Temporal Filtering Properties of Midbrain Neurons In Vivo. *Journal of Neuroscience* 17, 3815–3825.
583 doi:10.1523/JNEUROSCI.17-10-03815.1997
- 584 Gardner, D. (1989). Noise modulation of synaptic weights in a biological neural network. *Neural Networks*
585 2, 69 – 76. doi:https://doi.org/10.1016/0893-6080(89)90016-6
- 586 Geerts, H., Wikswa, J., van der Graaf, P. H., Bai, J. P., Gaiteri, C., Bennett, D., et al. (2020).
587 Quantitative Systems Pharmacology for Neuroscience Drug Discovery and Development: Current
588 Status, Opportunities, and Challenges. *CPT: Pharmacometrics & Systems Pharmacology* 9, 5–20.
589 doi:10.1002/psp4.12478
- 590 Gerstner, W., Kistler, W. M., Naud, R., and Paninski, L. (2014). *Neuronal dynamics: From single neurons*
591 *to networks and models of cognition and beyond* (Cambridge, UK: Cambridge University Press)
- 592 Goldental, A., Guberman, S., Vardi, R., and Kanter, I. (2014). A computational paradigm for dynamic
593 logic-gates in neuronal activity. *Frontiers in Computational Neuroscience* 8, 52. doi:10.3389/fncom.
594 2014.00052

- 595 Guillaumon, A., McLaughlin, D. W., and Rinzel, J. (2006). Estimation of synaptic conductances. *Journal of*
596 *Physiology-Paris* 100, 31 – 42. doi:<https://doi.org/10.1016/j.jphysparis.2006.09.010>. Theoretical and
597 Computational Neuroscience: Understanding Brain Functions
- 598 Hanisch, N. and Pierobon, M. (2017). Digital modulation and achievable information rates of thru-body
599 haptic communications. In *Disruptive Technologies in Sensors and Sensor Systems* (International Society
600 for Optics and Photonics), vol. 10206, 1020603
- 601 Hines, M., Davison, A., and Muller, E. (2009). NEURON and Python. *Frontiers in Neuroinformatics* 3, 1.
602 doi:10.3389/neuro.11.001.2009
- 603 Hodgkin, A. L. and Huxley, A. F. (1952). A quantitative description of membrane current and its application
604 to conduction and excitation in nerve. *The Journal of physiology* 117, 500–544
- 605 Hu, W. and Bean, B. P. (2018). Differential Control of Axonal and Somatic Resting Potential by Voltage-
606 Dependent Conductances in Cortical Layer 5 Pyramidal Neurons. *Neuron* 97, 1315 – 1326.e3. doi:<https://doi.org/10.1016/j.neuron.2018.02.016>
- 607
- 608 Jirsa, V. K., Stacey, W. C., Quilichini, P. P., Ivanov, A. I., and Bernard, C. (2014). On the nature of seizure
609 dynamics. *Brain* 137, 2210–2230. doi:10.1093/brain/awu133
- 610 Khodaei, A. and Pierobon, M. (2016). An intra-body linear channel model based on neuronal subthreshold
611 stimulation. In *2016 IEEE International Conference on Communications (ICC)*. 1–7. doi:10.1109/ICC.
612 2016.7511483
- 613 Koch, C. (2004). *Biophysics of Computation: Information Processing in Single Neurons* (New York:
614 Oxford University Press), chap. Linearizing Voltage-Dependent Currents. Computational Neuroscience.
615 232–247
- 616 Koslow, S. and Subramaniam, S. (2005). *Databasing the Brain: From Data to Knowledge*
617 *(Neuroinformatics)* (Wiley)
- 618 Larouche, J. and Aguilar, C. A. (2018). New technologies to enhance in vivo reprogramming for
619 regenerative medicine. *Trends in biotechnology*
- 620 Lienert, F., Lohmueller, J. J., Garg, A., and Silver, P. A. (2014). Synthetic biology in mammalian cells:
621 next generation research tools and therapeutics. *Nature Reviews Molecular Cell Biology* 15, 95–107.
622 doi:10.1038/nrm3738
- 623 Long, L. and Fang, G. (2010). A Review of Biologically Plausible Neuron Models for Spiking Neural
624 Networks. In *AIAA Infotech@Aerospace 2010* (America Institute of Aeronautics and Astronautics),
625 1–14. doi:10.2514/6.2010-3540
- 626 Markram, H. et al. (2015). Reconstruction and Simulation of Neocortical Microcircuitry. *Cell* 163,
627 456–492. doi:10.1016/j.cell.2015.09.029
- 628 Mauro, A., Conti, F., Dodge, F., and Schor, R. (1970). Subthreshold Behavior and Phenomenological
629 Impedance of the Squid Giant Axon. *The Journal of General Physiology* 55, 497–523. doi:10.1085/jgp.
630 55.4.497
- 631 Mishra, A. and Majhi, S. K. (2019). A comprehensive survey of recent developments in neuronal
632 communication and computational neuroscience. *Journal of Industrial Information Integration* 13, 40 –
633 54. doi:10.1016/j.jii.2018.11.005
- 634 Moreno-Bote, R. and Parga, N. (2004). Role of synaptic filtering on the firing response of simple model
635 neurons. *Phys. Rev. Lett.* 92, 028102. doi:10.1103/PhysRevLett.92.028102
- 636 Motanis, H., Seay, M. J., and Buonomano, D. V. (2018). Short-Term Synaptic Plasticity as a Mechanism for
637 Sensory Timing. *Trends in Neurosciences* 41, 701 – 711. doi:<https://doi.org/10.1016/j.tins.2018.08.001>.
638 Special Issue: Time in the Brain

- 639 Nise, N. S. (2015). *Control Systems Engineering* (California State Polytechnic University, Pomona: Wiley),
640 7 edn.
- 641 Peters, A. (2010). *The Morphology of Minicolumns* (Boston, MA: Springer US), chap. 4. 45–68.
642 doi:10.1007/978-1-4419-1272-5_4
- 643 Plesser, H. E. and Geisel, T. (1999). Bandpass properties of integrate-fire neurons. *Neurocomputing* 26-27,
644 229 – 235. doi:https://doi.org/10.1016/S0925-2312(99)00076-4
- 645 Pospischil, M., Toledo-Rodriguez, M., Monier, C., Piwkowska, Z., Bal, T., Frégnac, Y., et al. (2008).
646 Minimal Hodgkin–Huxley type models for different classes of cortical and thalamic neurons. *Biological*
647 *Cybernetics* 99, 427–441. doi:10.1007/s00422-008-0263-8
- 648 Rolston, J. D., Englot, D. J., Wang, D. D., Shih, T., and Chang, E. F. (2012). Comparison of seizure control
649 outcomes and the safety of vagus nerve, thalamic deep brain, and responsive neurostimulation: evidence
650 from randomized controlled trials. *Neurosurgical Focus FOC* 32, E14
- 651 Sabah, N. and Leibovic, K. (1969). Subthreshold Oscillatory Responses of the Hodgkin-Huxley Cable
652 Model for the Squid Giant Axon. *Biophysical Journal* 9, 1206 – 1222. doi:https://doi.org/10.1016/
653 S0006-3495(69)86446-5
- 654 Scharfman, H. E. (2007). The Neurobiology of Epilepsy. *Current Neurology and Neuroscience Reports* 7,
655 348–354. doi:10.1007/s11910-007-0053-z
- 656 Sengupta, B., Faisal, A. A., Laughlin, S. B., and Niven, J. E. (2013). The Effect of Cell Size and Channel
657 Density on Neuronal Information Encoding and Energy Efficiency. *Journal of Cerebral Blood Flow &*
658 *Metabolism* 33, 1465–1473. doi:10.1038/jcbfm.2013.103. PMID: 23778164
- 659 Veletić, M., Barros, M. T., Balasingham, I., and Balasubramaniam, S. (2019). A Molecular Communication
660 Model of Exosome-Mediated Brain Drug Delivery. In *Proceedings of the Sixth Annual ACM*
661 *International Conference on Nanoscale Computing and Communication* (New York, NY, USA:
662 Association for Computing Machinery), NANOCOM '19, 1–7. doi:10.1145/3345312.3345478
- 663 Vogels, T. P. and Abbott, L. F. (2005). Signal propagation and logic gating in networks of integrate-and-fire
664 neurons. *Journal of Neuroscience* 25, 10786–10795. doi:10.1523/JNEUROSCI.3508-05.2005
- 665 Wilson, C. J., Weyrick, A., Terman, D., Hallworth, N. E., and Bevan, M. D. (2004). A Model of
666 Reverse Spike Frequency Adaptation and Repetitive Firing of Subthalamic Nucleus Neurons. *Journal of*
667 *Neurophysiology* 91, 1963–1980. doi:10.1152/jn.00924.2003. PMID: 14702332
- 668 Zhou, Y., Peng, Z., Seven, E. S., and Leblanc, R. M. (2018). Crossing the blood-brain barrier with
669 nanoparticles. *Journal of Controlled Release* 270, 290 – 303. doi:https://doi.org/10.1016/j.jconrel.2017.
670 12.015